New p-type Al-substituted SrSnO 3 perovskites for TCO applications?

Leila Ben Amor, Besma Belgacem, Jean-Sébastien Filhol, Marie-Liesse
Doublet, Mouna Ben Yahia, Rached Ben Hassen

HAL Id: hal-02519420

https://hal.umontpellier.fr/hal-02519420

Submitted on 6 Nov 2020

New p-type Al-substituted SrSnO$_3$ perovskite for TCO applications?

Leila Ben Amor,[a][b] Besma Belgacem,[a] Jean-Sébastien Filhol,[b] Marie-Liesse Doublet,[b] Mouna Ben Yahia*[b] and Rached Ben Hassen[a]

Novel p-type SrSn$_{1-x}$Al$_x$O$_3$ (x=0, 0.2, 0.5) perovskites are presented as potential candidates for electro-optical applications. A combined experimental and theoretical study reveals that chemical substitutions can be used as a lever to stabilize oxygen holes in the valence band.

Transparent conductive oxides (TCO) are an original class of materials combining two contrasting properties in one single compound that is, electrical conductivity and optical transparency in visible spectrum. TCOs are widely used in electro-optical devices such as flat-panels, organic light emitting diodes, photovoltaic devices, and plasma displays.[1–6] However, standard commercial TCOs are limited to post-transition metal oxides, e.g. ZnO, In$_2$O$_3$ and SnO and derivatives.[7] These oxides are characterized by a band gap larger than 3eV between the O$(2p)$ valence band maximum (VBM) and the metal (s,p) conduction band minimum (CBM). They display excellent n-type electronic conductivity when the donor, i.e. metal, is doped. In contrast, the development of high performant p-type TCOs is more challenging,[8–11] due to the strongly localized states of the acceptor, i.e. oxygen, which are at the origin of large hole effective mass (poor electronic conductivity). As a consequence, the probability is high that the newly created shallow acceptors are counterbalanced by the formation of native defects such as anion vacancies or cation interstice.[12] Up to now, n-type tin-doped indium oxide (ITO) shows the best performance.[1,13] Nevertheless and despite the remarkable properties of ITO, the relative high cost of In and its increasing scarcity appeals for alternative elements or materials.[14] ABO$_3$ perovskites are of great interest thanks to the use of mixed A and B cations capable of generating versatile structures and properties with high chemical stability. SrSnO$_3$ (SSO) is one of the most promising candidate due to its high visible light transmittance, high thermal stability and reasonable cost.[15] Pure SSO is a charge transfer insulator crystallizing in the orthorhombic GdFeO$_3$-type structure with lattice parameters a = 5.7113 Å, b = 8.0647 Å and c = 5.7042 Å. In this tri-dimensional structure, SnO$_6$ octahedra are corner-shared and Sr lies in the available vacant interstices.[16,17] To meet the industrial specifications of efficient TCOs, SSO must display high carrier concentration and mobility[18–21] which requires its doping. Attempts to develop n-type SSO candidates that could rival the electro-optical properties of ITO were intensively described and interesting performance were reported.[22–26] In contrast, p-type doping is still lacking for this class of materials.[27–29] Recently, Hautier *et al.* showed that the large difference in mobility between n-type and p-type materials is not inevitable and could be overcome by the investigation of alternative chemistries. Based on this statement and considering the high industrial stakes associated with the discovery of new p-type TCOs, we used chemical substitution to check the ability of SSO to behave as a performant p-type TCO. This concept was introduced for the first time by Hosono and coworkers[2] and is known as the "chemical modulation of the valence band" (CMVB). Based on the hypothesis that partial substitution of Sn(IV) for the smaller trivalent cation Al(III) can enhance electron delocalization (through a significant volume contraction of the perovskite structure) while concomitantly generate stable holes in the valence band, various Sn/Al-substituted SSO phases were synthesized. Using X-ray diffraction (XRD) and Scanning Electron Microscopy (SEM) equipped with Energy Dispersive X-ray Spectroscopy (EDX), we here demonstrate the solubility of the Al element in the SSO perovskite structure for SrSn$_{1-x}$Al$_x$O$_3$ (SSAO) compositions x = 0 to 0.5. UV-Vis-NIR spectroscopy is then used to show that the absorption profile of SSO is not altered by the chemical Sn/Al substitution while the low-energy absorption band (intra-band transitions) is enhanced. A thermodynamic study based on first-principles DFT (Density Functional Theory) calculations is then performed to determine the type of charge carriers in SSO and SSAOs (p-type) and combined with chemical bond analyses to rationalize the impact of Sn/Al substitution on the p-type performance of SSAOs.

SrSn$_{1-x}$Al$_x$O$_3$ (x= 0, 0.2, 0.5) perovskites were successfully obtained through solid state reaction. Details of the synthesis steps are given in ESI part. The impact of the Sn(IV)/Al(III) substitution ratio on the macroscopic properties of SrSn$_{1-x}$Al$_x$O$_3$ was investigated through complementary XRD and SEM-EDX. The structural and morphological analyses of the synthesized samples are presented in Fig.1 and S1. From the XRD patterns of SSO and SrSn$_{1-x}$Al$_x$O$_3$ (SSAO) the orthorhombic Pnma structure (JCPDS 10–6354) is confirmed. A slight shift towards higher angles is observed in agreement with the smaller Shannon ionic radius of Al^{3+} (0.54 Å) compared to Sn^{4+} (0.69 Å).

[a.] *Laboratoire des Matériaux et de l'environnement pour le Développement Durable LR18ES10, ISSBAT, Université de Tunis El Manar 9, Avenue Dr. Zoheir Safi, 1006 Tunis, Tunisia.*
[b.] *Institut Charles Gerhardt, Univ. Montpellier, CNRS, ENSCM, Montpellier, France*
* mouna.ben-yahia@umontpellier.fr
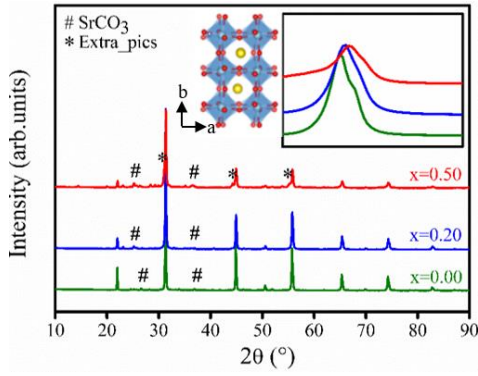
Figure 1 X-ray diffraction patterns and enlargement at $2\theta \sim 31°$ and of $SrSn_{1-x}Al_xO_3$ (x=0, 0.20 and 0.50)

Figure 2 (a) UV-Vis-NIR absorption spectra and (b) optical band gap estimation using Tauc's formula $(\alpha h \upsilon)^2 = f(h\upsilon)$ of $SrSnO_{1-x}Al_xO_3$ (x=0, 0.20 and 0.50).

For all compositions, the Goldschmidt tolerance (t) and distortion octahedral (μ) factors remain in the range [0.8-1.1][30] and [0.41-0.73], respectively.[31,32] which confirms the phase stability. Note that a small amount of $SrCO_3$ impurity was detected and attributed to the potential reaction of Sr defects with atmospheric oxygen and carbon dioxide.[33] This is confirmed by DFT calculations showing that the formation of $SrCO_3$ from SSO is favoured for all compositions (see Table S1). Interestingly, the content of $SrCO_3$ impurities slightly decreases with the increase of Sn/Al ratio (xAl_{Sn}). This suggests that Sr vacancies are less favoured in SSAO as xAl_{Sn} increases, as confirmed by DFT calculations (see Table S1). For xAl_{Sn} = 0.5, extra reflections appear in the XRD patterns that could be assigned to either a superstructure, or the formation of a cubic-type structure as previously reported by Waerenborgh and coworkers for xAl_{Fe}=0.5 substitution in $SrFe_xAl_{1-x}O_3$.[34] Structural predictions carried out by means of a basing-hopping procedure clearly identify cubic SSAOs as thermodynamically favoured over orthorhombic polymorph when xAl_{Sn} reaches x=0.5. This could arise from an Al ordering occurring in the structure (see Fig. S2). The magnified scanning electron microscopy (SEM) images and energy dispersive x-ray (EDX) cartographies given in supplementary information (Fig. S1) show the formation of micron-sized agglomerates of raw elements Sr, Sn, Al and O. An additional carbon peak is also observed which originates from the sampling method that uses graphite film deposit. Interestingly, when measurements are performed on pellet, the carbon signature drastically decreases and $SrCO_3$ impurities remain as trace (see Fig. S1d).

UV-Vis-NIR Optical reflectance was further measured for each sample up to 2700 nm (Fig. 2a). All spectra are similar and show two distinct zones: one strong optical absorption zone in the range 270-400 nm, which is attributed to the transition from the VBM (predominant O(2p) states) to the CBM (predominant Sn(5s,p)). Wide and less intense bands are then observed around 500 nm that can be assigned to carbonate-type impurities (known to absorb in that region[35]). The amplitude of these bands decreases with the increase of xAl_{Sn}, consistently with the progressive decrease of the amount of $SrCO_3$ impurity. Interestingly, additional peaks are observed in the 1400-2700 nm NIR region which were not reported in the literature, even for the un-doped SSO material. The shape of these peaks is very similar for SSO and SSAO suggesting equivalent intra-band electronic transitions and equivalent type of charge carriers for all compositions. Noteworthy, the width and intensity of these transitions is directly correlated to the Sn/Al substitution ratio. This absorption continuum indicates interesting conducting
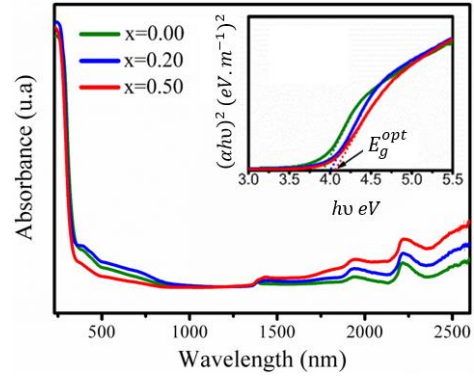
properties, possibly associated with shallow acceptor states (i.e. stable oxygen-holes) in the valence band, both for unsubstituted SSO and substituted SSAOs. To determine which charge carriers occur in SSAOs (n- or p-type), electronic conductivity and Seebeck (or Hall-effect) measurements are necessary. However, such measurements require high-temperature sintering techniques to get high-density samples. This procedure is known to induce undesired O_2 release that can switch transport properties from p- to n-type, therefore leading to unreliable results.[36] Indeed, the main impediment to p-doping in oxides has been identified as the formation of compensating intrinsic defects (hole killers) such as oxygen vacancies.[12,37,38] The occurrence of stable oxygen vacancies (V_O) is then not desired as they may kill the shallow acceptor states created by Sr-defects or Al_{Sn} substitution. In contrast, native defects of cations such as Sr (V_{Sr}) and Sn (V_{Sn}) are beneficial for p-type behavior. It is therefore crucial to determine the nature of the defects in the SSO and SSAO structures in order to properly assign the low-energy transitions observed in their absorption spectra. For this propose, a thermodynamic DFT study was conducted for the substituted SSAO phases to assess the stability of the oxygen network towards O_2 gas release, with and without the presence of Sr vacancies.

$$Sr_{1-y}Sn_{1-x}Al_xO_3 \rightarrow Sr_{1-y}Sn_{1-x}Al_xO_{3-\delta} + \left(\frac{\delta}{2}\right)O_2 \quad (1)$$
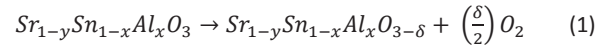
According to reaction (1), a direct relation can be established between y, x and δ to identify the doping-type of the material. A p-type behavior (resp. n-type) is expected for $y + \frac{x}{2} > \delta$ (resp. $< \delta$) i.e. when the charge compensation due to Sr vacancies and Sn/Al substitutions remains greater (resp. lower) than the content of released O_2. The frontier between both regimes is illustrated by a dashed line in Fig. 3 and corresponds to a number of holes per O of 0.087. Remarkably, the reaction enthalpy remains positive up to 0.13 holes per oxygen, which suggests that p-type SSAOs could be stable in a narrow domain of O-holes from 0.087 to 0.13, with no oxygen release. Above this critical value, O_2 is released but the system remains p-type ($\delta < y + \frac{x}{2}$) up to 0.22 holes per oxygen. Optical band gaps (E_g^{opt}) were extracted from the absorption spectra using Tauc's theory[39] (see section Methods in ESI) and are displayed in Fig.2b. The extrapolation of the straight line portion of the $(\alpha h v)^2$ plots to α= 0 gives a good estimates of E_g^{opt} values. They correspond to 3.9, 4.0 and 4.1 eV for xAl_{Sn}=0, 0.2 and 0.5, respectively, in good agreement with the literature for SSO.[40,41]
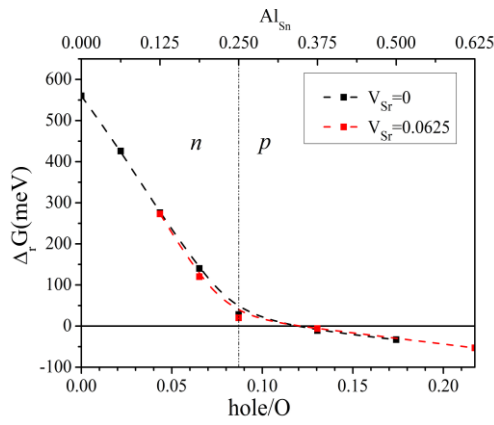
Figure 3: Stability of the oxygen network towards oxygen vacancies V_O ($V_O = \delta = 0.125$) with and without the presence of Sr vacancies V_{sr} ($V_{sr} = y = 0.0625$). The xAl_{Sn} composition scale is given for the black curve. The Al ratio for the red curve is equal to $xAl_{Sn} - 2y$. The charge carrier type is defined by the sign of the relation $(2y+x)-2\delta$. Dashed line delimits the n/p-type charge carriers.

These results clearly predict a stability domain for p-type conduction due to chemical substitution.

The band structures computed for SSO and SSAO ($xAl_{Sn}=0.25$) are presented in Figs.4a, b. SSO shows an indirect band gap between $U(1/2,0,1/2)$ and $\Gamma(0,0,0)$ consistent with previous reports.[41,42] Interestingly, SSAO displays a direct band gap around Γ showing that the symmetry lowering due to Sn/Al substitution does affect the general shape of the band structure. The computed band gaps are found to be 4.3 and 4.6 eV, for SSO and SSAO with $xAl_{Sn} = 0.25$, respectively, in good agreement with recent calculations using the hybrid HSE (Heyd–Scuseria–Ernzerhof) functional,[43] and in fairly good accordance with the experimental blue-shift observed in Fig. 2b. The shallow states observed at the VBM of SSAO increase with the Sn(IV)/Al(III) substitution ratio. According to the projected Density of States (DOS) these states are assigned to the oxygen atoms that are directly connected to Al (Fig. S4). This is fully consistent with the less efficient electrostatic stabilization of O^{2-} anions by Al^{3+} compared to Sn^{4+}.[44] The comparison of the electronic band structures of Figs. 4a and b highlights a perturbation of the electronic states of SSAO compared to SSO and a substantial increase of the valence bandwidth. To quantify the VBM dispersion and transport properties, anisotropic hole effective masses were evaluated for SSAO by measuring the band curvature around Γ, Y and Z, as well as along the most interesting Γ-X (½, 0, 0), $Y(0, ½, 0)$-$M(½,½,0)$ and $Z(0, 0, ½)$ -$R(0, ½, ½)$ directions of the Brillouin zone (See Fig. S5). Results give ~$0.62m_e$, ~$0.43m_e$ and ~$0.67m_e$ for SSAO and ~$0.80m_e$, ~$0.50m_e$ and ~$1.76m_e$ for SSO, respectively, showing that SSAO ($xAl_{Sn}=0.25$) displays lower effective masses than SSO for a given direction. Heavier effective mass is obtained on U and along U-Γ direction ($1.34m_e$ for SSAO and $4.77m_e$ for SSO). This can be fully rationalized via chemical bond analyses through the computation of Fukui functions (f^-) and electron localization functions (ELF). As detailed in SI, these topological tools of the electron density provide direct proves of the VBM states (Fukui) and real-space Lewis-like structures (ELF). The Fukui functions of SSO and SSAO reveal that the VBM states have an oxygen character with, however, very different spatial distributions for both systems. While SSO shows O($2p$) orbitals perpendicular to the (a,c) plane, a more spherical density is clearly visible around the oxygens for
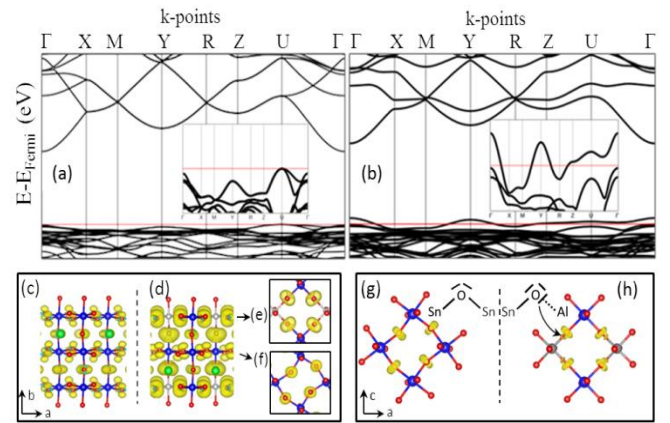
Figure 4: Band structures computed for (a) SrSnO$_3$ and (b) SrSn$_{0.75}$Al$_{0.25}$O$_3$ and their magnification (insets) in the range of 1 eV around the Fermi level (red horizontal line). Fukui functions of (c) SrSnO$_3$ and (d) SrSn$_{0.75}$Al$_{0.25}$O$_3$ projected in the ab plane where Sn, Al and O are represented in blue, grey and red, respectively. (e) Fukui function of SrSn$_{0.75}$Al$_{0.25}$O$_3$ in the mixed Sn/Al and pure Sn planes (ac plane). ELF functions and the corresponding Lewis representations of Sn-O-M (M=Sn or Al) bridge of (g) SrSnO$_3$ and (h) SrSn$_{0.75}$Al$_{0.25}$O$_3$.

SSAO, indicative of an enhanced Sn-O bond covalency (Figs. 4c-d). The ELF plots of Fig. 4g-h show that two oxygen lone-pairs pointing towards the Sr^{2+} cations (two yellow volumes) for both SSO and SSAO. They correspond to the O($2s$) and O($2p$) lone-pairs of oxygens that are not involved in covalent bonds with Sn or Al and are consistent with the oxygen Lewis structure that is expected in such local environment (see Fig. 4g). Interestingly, another lobe is visible along the Al-O bonds but close to O, which illustrates a loss of Al-O interactions in the lattice, fully consistent with the less electronegative character of Al with respect the Sn (Fig. 4h). Owing to the smaller radius of Al compared to Sn, the Al/Sn substitution induces a significant contraction of the Sn-O bonds, from 2.08 to 2.04 Å and a substantial O-Sn-O angle increase from 155° to 175° which both contribute to the increase of the valence band width (Fig. 4d). These local distortions impact the cell parameters of SSAO which notably contract in the (a,c) plane, a=5.635 Å, b=8.114 Å and c=5.614 Å (c/b=0.69) for $xAl_{Sn}=0.25$. The decrease of the c/b ratio is in line with the increase of the Goldschmidt tolerance factor t (t = 0.96 for SSO and 0.98 for $xAl_{Sn}=0.25$) and the progressive orthorhombic to cubic phase transition predicted for large xAl_{Sn} contents. Overall, this study shows that the increase of the valence band width with xAl_{Sn}, which is a desired outcome for p-type TCO materials, results from the substantial increase in Sn-O covalency associated with a negative Moss-Burstein shift (creation of O hole) in the VBM.

In summary, new p-type SrSn$_{1-x}$Al$_x$O$_3$ (x = 0, 0.2 and 0.5) perovskites have been successfully synthesized using solid state reaction. The comparison of UV-visible-NIR absorption spectra of SSO and SSAO reveals two important features: 1) an increase in the optical band gap (>3.9 eV) together with the persistence of transparency and 2) the onset of NIR electronic transitions (1400-2700 nm) that increases with xAl_{Sn}. DFT calculations predict a thermodynamic stability domain for p-type charge carriers in SSAOs, which increases with the Sn/Al substitution ratio. The Sn/Al substitution leads to an increase in the Sn-O bond covalency in conjunction with the creation of stable O-holes in the top portion of the valence band. Despite our unsuccessful attempts to carry out electrical

conductivity measurements, we believe the structure/property correlation established in this work gives a body of evidence that SSAO materials do behave as p-type transparent conductive oxides. Work is in progress to conclude on that point with thin-film formulation being sought as an alternative to powder synthesis to assess transport properties of SSAO materials. To conclude, chemical substitutions rather than doping give hopes that environmental friendly p-type materials could compete with current n-type materials for TCO applications. The richness of the metal oxide family of compounds provides solid state chemists for an amazing playground to search for the winning combination of elements.

Conflicts of interest

There are no conflicts to declare.

Notes and references

1 H. Ohta, M. Orita, M. Hirano, H. Tanji, H. Kawazoe and H. Hosono, *Appl. Phys. Lett.*, 2000, **76**, 2740–2742.
2 H. Hosono, *Proc. Sympodium O Thin Film Chalcogenide Photovolt. Mater. EMRS 2006 Conf.*, 2007, **515**, 6000–6014.
3 E. Fortunato, P. Barquinha and R. Martins, *Adv. Mater.*, 2012, **24**, 2945–2986.
4 C. G. Granqvist, *Sol. Energy Mater. Sol. Cells*, 2007, **91**, 1529–1598.
5 L. Escoubas, J. J. Simon, J. Le Rouzo and V. Bermudez, in *Optical Thin Films and Coatings*, eds. A. Piegari and F. Flory, Woodhead Publishing.
6 E. Fortunato, D. Ginley, H. Hosono and D. C. Paine, *MRS Bull.*, 2007, **32**, 242–247.
7 T. Minami, *Semicond. Sci. Technol.*, 2005, **20**, S35–S44.
8 G. Hautier, A. Miglio, G. Ceder, G.-M. Rignanese and X. Gonze, *Nat. Commun.*, 2013, **4**, 2292.
9 R. Woods-Robinson, D. Broberg, A. Faghaninia, A. Jain, S. S. Dwaraknath and K. A. Persson, *Chem. Mater.*, 2018, **30**, 8375–8389.
10 N. Sarmadian, R. Saniz, B. Partoens and D. Lamoen, *Sci. Rep.*, 2016, **6**, 20446.
11 K. H. L. Zhang, K. Xi, M. G. Blamire and R. G. Egdell, *J. Phys. Condens. Matter*, 2016, **28**, 383002.
12 A. Zunger, *Appl. Phys. Lett.*, 2003, **83**, 57–59.
13 R. Bel Hadj Tahar, T. Ban, Y. Ohya and Y. Takahashi, *J. Appl. Phys.*, 1998, **83**, 2631–2645.
14 G. S. Selopal, R. Milan, L. Ortolani, V. Morandi, R. Rizzoli, G. Sberveglieri, G. P. Veronese, A. Vomiero and I. Concina, *Sol. Energy Mater. Sol. Cells*, 2015, **135**, 99–105.
15 M. A. Riza, M. A. Ibrahim, U. C. Ahamefula, M. A. M. Teridi, N. A. Ludin, S. Sepeai and K. Sopian, *Sol. Energy*, 2016, **137**, 371–378.
16 A. Vegas, M. Vallet-Regi, J. M. Gonzalez-Calbet and M. A. Alario-Franco, *Acta Crystallogr. Sect. B*, 1986, **42**, 167–172.
17 S. Ouni, S. Nouri, J. Rohlicek and R. B. Hassen, *J. Solid State Chem.*, 2012, **192**, 132–138.

18 D. Segev and S.-H. Wei, *Phys Rev B*, 2005, **71**, 125129.
19 H. Mizoguchi and P. M. Woodward, *Chem. Mater.*, 2004, **16**, 5233–5248.
20 H. Mizoguchi, H. W. Eng and P. M. Woodward, *Inorg. Chem.*, 2004, **43**, 1667–1680.
21 P. M. Woodward, H. Mizoguchi, Y.-I. Kim and and M. W. Stoltzfus, The Electronic Structure of Metal Oxides.
22 Q. Liu, J. Dai, X. Zhang, G. Zhu, Z. Liu and G. Ding, *Thin Solid Films*, 2011, **519**, 6059–6063.
23 Q. Liu, H. Li, B. Li, W. Wang, Q. Liu, Y. Zhang and J. Dai, *EPL Europhys. Lett.*, 2014, **108**, 37003.
24 Q. Liu, F. Jin, G. Gao and W. Wang, *J. Alloys Compd.*, 2017, **717**, 62–68.
25 Q. Liu, B. Li, H. Li, K. Dai, G. Zhu, W. Wang, Y. Zhang, G. Gao and J. Dai, *Jpn. J. Appl. Phys.*, 2015, **54**, 031101.
26 E. Baba, D. Kan, Y. Yamada, M. Haruta, H. Kurata, Y. Kanemitsu and Y. Shimakawa, *J. Phys. Appl. Phys.*, 2015, **48**, 455106.
27 Z. Wang, P. K. Nayak, J. A. Caraveo-Frescas and H. N. Alshareef, *Adv. Mater.*, 2016, **28**, 3831–3892.
28 K. Fleischer, E. Norton, D. Mullarkey, D. Caffrey and I. V. Shvets, *Materials*, 2017, **10**, 1019.
29 K. H. L. Zhang, K. Xi, M. G. Blamire and R. G. Egdell, *J. Phys. Condens. Matter*, 2016, **28**, 383002.
30 V. M. Goldschmidt, *Naturwissenschaften*, 1926, **14**, 477–485.
31 Z. L. Wang and K. C. Kang, *Functional and Smart Materials*, New York, London, Plenum Press.
32 S. Zhu, J. Ye, Y. Zhao and Y. Qiu, *J. Phys. Chem. C*, 2019, **123**, 20476–20487.
33 G. L. Lucena, J. J. N. Souza, A. S. Maia, L. E. B. Soledade, E. Longo, A. G. Souza and I. M. G. Santos, *Cerâmica*, 2013, **59**, 249–253.
34 J. C. Waerenborgh, D. P. Rojas, A. L. Shaula, G. C. Mather, M. V. Patrakeev, V. V. Kharton and J. R. Frade, *Mater. Lett.*, 2005, **59**, 1644–1648.
35 M. Saleem, N. G. Choi and K. H. Lee, *Int. J. Environ. Anal. Chem.*, 2015, **95**, 592–608.
36 S. Singh, P. Singh, O. Parkash and D. Kumar, *Adv. Appl. Ceram.*, 2007, **106**, 231–234.
37 J. Robertson and S. J. Clark, *Phys. Rev. B*, 2011, **83**, 075205.
38 D. O. Scanlon and G. W. Watson, *J. Mater. Chem.*, 2012, **22**, 25236–25245.
39 J. Tauc, R. Grigorovici and A. Vancu, *Phys. Status Solidi B*, 1966, **15**, 627–637.
40 B. Bellal, B. Hadjarab, A. Bouguelia and M. Trari, *Theor. Exp. Chem.*, 2009, **45**, 172–179.
41 T. Schumann, S. Raghavan, K. Ahadi, H. Kim and S. Stemmer, *J. Vac. Sci. Technol. A*, 2016, **34**, 050601.
42 K. P. Ong, X. Fan, A. Subedi, M. B. Sullivan and D. J. Singh, *APL Mater.*, 2015, **3**, 062505.
43 C. Wang, Y. Liu, Y. Lu, P. Wu and W. Zhou, *Comput. Mater. Sci.*, 2018, **145**, 102–108.
44 M. Ben Yahia, J. Vergnet, M. Saubanère and M.-L. Doublet, *Nat. Mater.*, 2019, **18**, 496–502.